Supporting Information

First-principles study of interfacial features and charge dynamics between Spiro-MeOTAD and photoactive lead halide perovskites

Adriana Pecoraro,[a] Francesca Fasulo,[b] Michele Pavone[b,c] and Ana B. Muñoz-García[a,c,*]

a) Department of Physics "E. Pancini", University of Naples Federico II, Napoli, Italy
b) Department of Chemical Sciences, University of Naples Federico II, Napoli, Italy
c) National Reference Center for Electrochemical Energy Storage (GISEL)-INSTM, Florence, Italy
* Corresponding author: anabelen.munozgarcia@unina.it

Computational Details

We performed DFT [S1] calculations with periodic boundary conditions (PBC) employing the light–tier1 basis set of numerical atom-centered orbitals (NAO) for each atom [S2] for geometry optimization and electronic analysis, respectively, as implemented in the Fritz Haber Institute ab initio molecular simulations (FHI-aims) code [S3]. Within the FHI-aims framework, the electrons were described by the zero–order regular approximation (atomic ZORA)[S4]. As self-consistency threshold for electron density convergence, we employed a total energy criterion of 1×10^{-6} eV. We used the Perdew-Burke-Erzenhof (PBE) [S5,S6] exchange correlation functional for all geometry optimizations including the Tkatchenko–Scheffler (TS) correction [S7] accounting for van der Waals dispersion forces. During geometry optimizations involving the perovskite surface, atoms of the bottommost layers have been fixed to their bulk-like positions, while the first layer and the adsorbed molecule have been allowed to relax without symmetry constraints. Our relaxed structures present maximum forces acting on each atom below 0.05 eV/Å. Due to large dimensions of the bulk and the surfaces, the gamma point (1×1×1) k-point sampling scheme was applied for all calculations. The pDOS of the investigated perovskite/Spiro-MeOTAD interfaces have been made with FHI-AIMs with HSE06 functional [S8] and light–tier1 basis set. We have computed the donor-acceptor couplings at HSE06 level of theory, as implemented by Futera *et al.* [S9] in the CP2K software [S10]. Electron (hole) injection times have been calculated from coupling matrix elements within a theoretical framework involving a simple donor-acceptor model. Such model relies on the definition of charge-localized diabatic states that can be obtained through the projection-operator diabatization (POD) approach [S9]. This scheme consists in partitioning the Hilbert space of the system into a donor and an acceptor part and a separately diagonalization of the Hamiltonian matrix blocks so to define donor and acceptor states and the relative donor-acceptor couplings. Double-ζ basis functions with one set of polarization functions (double-ζ valence polarized (DZVP)) were used as basis sets with a plane wave cutoff of 300 Ry. The

Goedecker−Teter−Hutter (GTH) pseudopotentials were used to treat the core electrons, while the considered valence electrons are Pb:$6s^2 6p^2$, I:$5s^2 5p^5$, Br:$4s^2 4p^5$, O:$2s^2 2p^4$, N:$2s^2 2p^3$, H:$1s^1$, Cs:$5s^2 5p^6 6s^1$.

A safe transition between the two codes is ensured by the pDOS shown in Figure S6, which is qualitatively and quantitative similar for both codes.

Structural model of perovskites: Bulk structures and surface terminations.

Our study starts from building suitable computational models for the involved materials. The bulk structure of both triLHP and MAPI used in this work contains 100 $APbX_3$ perovskite f.u. and has been built by scaling back the $Cs_8FA_{88}MA_{12}Pb_{103}Cd_5I_{269}Br_{55}$ supercell (108 f.u.) reported by Saidaminov [S11], where Cs/FA/MA and I/Br are distributed randomly, and the orientation of the organic cations is determined by means of NVT molecular dynamics simulations. Besides resizing the supercell, all Cd sites have been replaced by Pb. For MAPI, all "A" sites have been substituted by randomly oriented MA and all "X" sites feature iodine, for a resulting $MA_{100}Pb_{100}I_{300}$ supercell. For triLHP, proper substitution on "A" and "X" sites have been made to obtain the desired stoichiometry in a $Cs_5FA_{79}MA_{16}Pb_{100}I_{250}Br_{50}$ supercell. Relaxed bulk structures and calculated lattice constants, together with the corresponding atom-projected density of states (pDOS), are reported in Figure S1. In agreement with literature [S12], introduction of Cs and large FA cations increases of ~1Å the lattice constants in triLHP with respect to MAPI and widens the band gap value of about ~0.09 eV, while preserving the species composition of the frontier bands. Starting coordinates for isolated Spiro-MeOTAD have been taken from a previous work [S13].

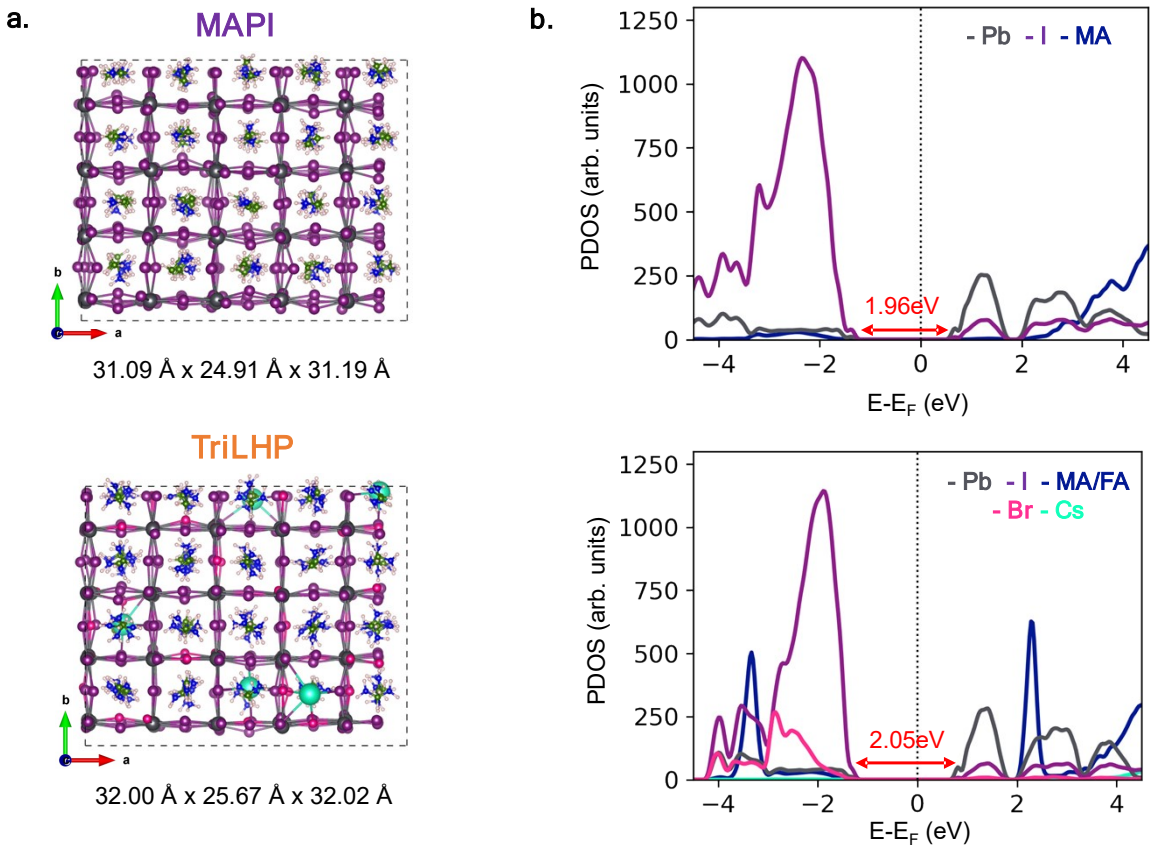

Figure S1. (a) Optimized structures and **(b)** projected density of states (pDOS) at PBE-TS level of theory of perovskite MAPI (top) and $Cs_{0.05}(FA_{0.83}MA_{0.17})_{0.95}Pb(I_{0.83}Br_{0.17})_3$ (bottom) bulk. Atomic color code: Cs (cyan), Br(magenta), I (violet), Pb (gray), C (green), N (blue), H (pink). pDOS color code: Cs (cyan), Br(magenta), I (violet), Pb (gray), MA/FA (green).

LHP/Spiro-MeOTAD interface models consist of a Spiro-MeOTAD molecule lying on a stoichiometric 8-layer thick surface slabs, cleaved from each LHP bulk along the most stable (010) plane [S14]. Addition of 25 Å vacuum prevents unphysical effects due to image interactions. We have considered both AX (A=MA in MAPI or Cs,FA,MA in triLHP) and PbX_2 terminations (X=I in MAPI or I, Br in triLHP). Our choice responds to two indications: first, surface termination has been found to influence the energy of Spiro-MeOTAD frontiers orbitals [S15]; second we are interested in the specific interaction occurring at interfaces that depends on the local chemical environment. While it is generally reported that AX-terminated surfaces are more stable than PbX_2 ones [S15], reaction conditions can change the chemical potential during film growth and there is a window under thermodynamic equilibrium where both terminations coexist [S16].

As shown by Figure S2, the specific physico-chemical effect of Cs is examined in depth by considering different compositions of the surface layer AX terminations in triLHP, i.e. exposing or not Cs atoms, labeled as CsFAMAX and FAMAX in the text, respectively. An additional CsFAMAX layer with maximized interaction of Cs with the most active methoxy groups of Spiro-MeOTAD [S17, S18] has been considered and labeled CsFAMAX(O-Cs). Similarly, we have investigated two different PbX_2-terminated surfaces, lacking or containing Cs atom in the subsurface layer, labeled as PbX_2 and PbX_2(Cs) in the text, respectively.

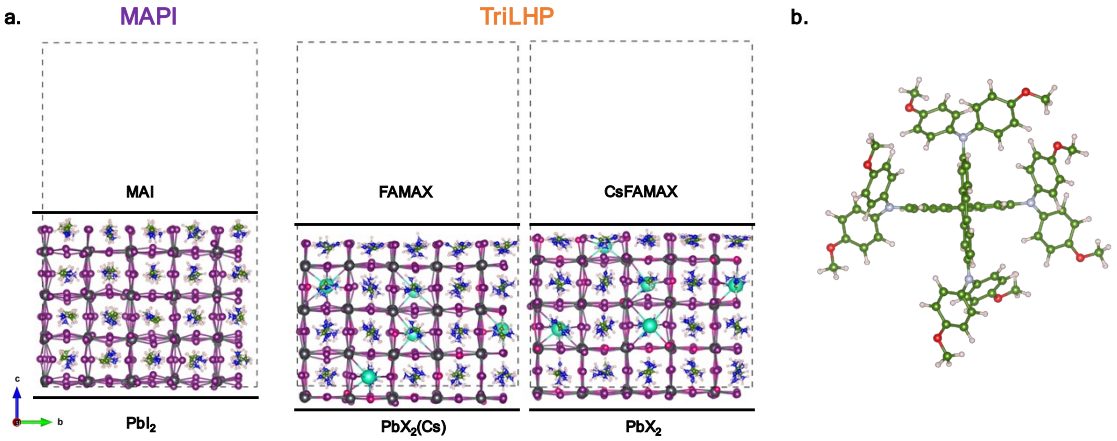

Figure S2. (a) Slab models of the surfaces considered for Spiro-MeOTAD adsorption on MAPI: MAI, PbI_2 and on triple cation FAMAX, PbX_2 (Cs) and CsFAMAX, PbX_2. **(b)** PBE-TS relaxed geometry of the Spiro molecule.

Structural and electronic analysis on perovskite/Spiro-MeOTAD interfaces

LHP/Spiro-MeOTAD interfacial distances have been evaluated as:

$$\bar{d}_{(Spiro-Surf),z} = \bar{z}_{Spiro} - \bar{z}_{Surf}$$

The first term $\bar{z}_{Spiro}$, is the average value of the z coordinates of Spiro-MeOTAD atoms belonging to a 1Å window from the Spiro-MeOTAD atom closest to the perovskite while $\bar{z}_{Surf}$ is the average value of the z coordinates of the perovskite atoms in the topmost layer. A graphical representation of the atoms involved in calculation of distances is shown in Figure S3.

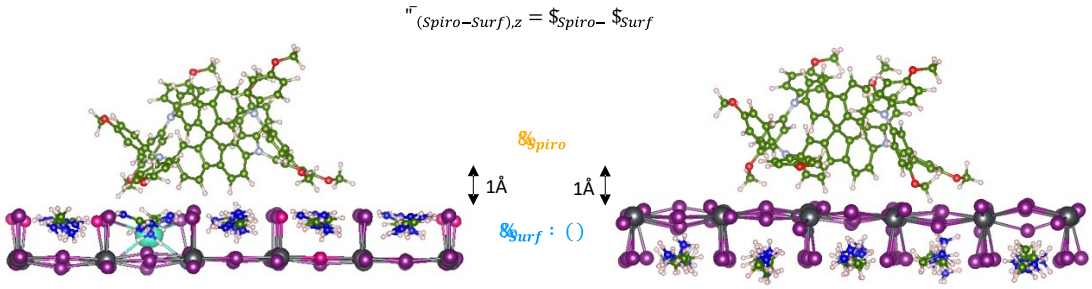

Figure S3: Graphical representation of layers that define distances reported in Table S1. Atoms in the blue and yellow regions are the one involved in calculation of distances for the surface and molecule, respectively.

Correlation of binding energies and interfacial distances can be evinced from data in Table S1.

Table S1. HSE06-TS values of the binding energies (E_b) of LHP/Spiro-MeOTAD interfaces with AX- or PbX_2- type terminations with different compositions, and average distances along z-axis between Spiro-MeOTAD and the topmost surfaces layer ($\bar{d}_{(Spiro-Surf),z}$).

AX-type	**MAI**	**FAMAX**	**CsFAMAX**	**CsFAMAX(O-Cs)**
E_b (eV)	-2.24	-1.99	-1.42	-2.25
$\bar{d}_{(Spiro-Surf),z}$(Å)	1.62	2.21	2.39	1.71
PbX_2-type	**PbI_2**	**PbX_2**	**PbX_2(Cs)**	
E_b (eV)	-1.94	-2.44	-3.02	
$\bar{d}_{(Spiro-Surf),z}$(Å)	2.00	1.58	1.50	

Analysis of structural distortions on Spiro-MeOTAD and LHP surfaces upon interface formation

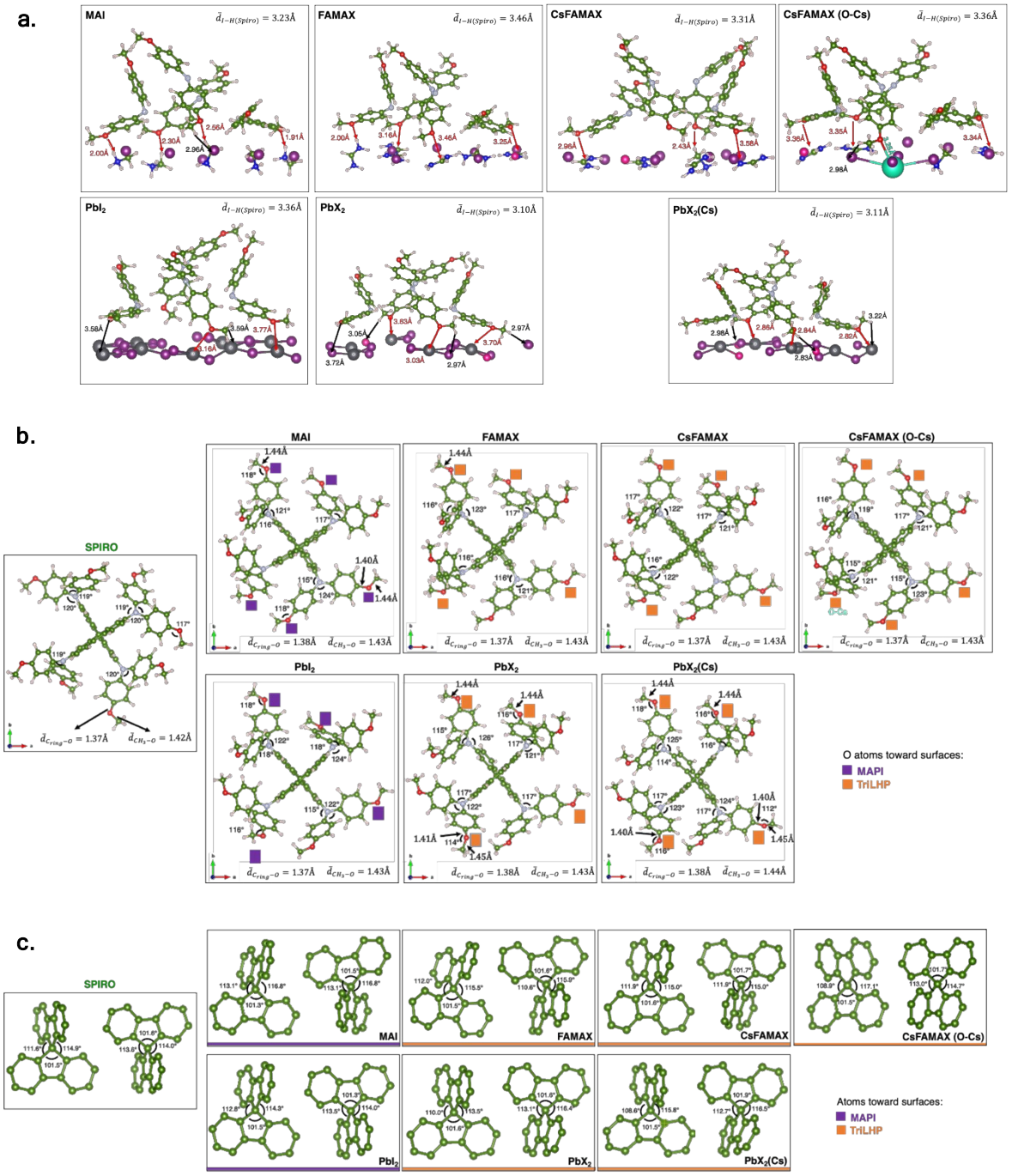

Figure S4: Main bond distances between Spiro-MeOTAD and surfaces **(a).** Structural variations of bond distances **(b)** and angles **(c)** of Spiro-MeOTAD upon interface formation.

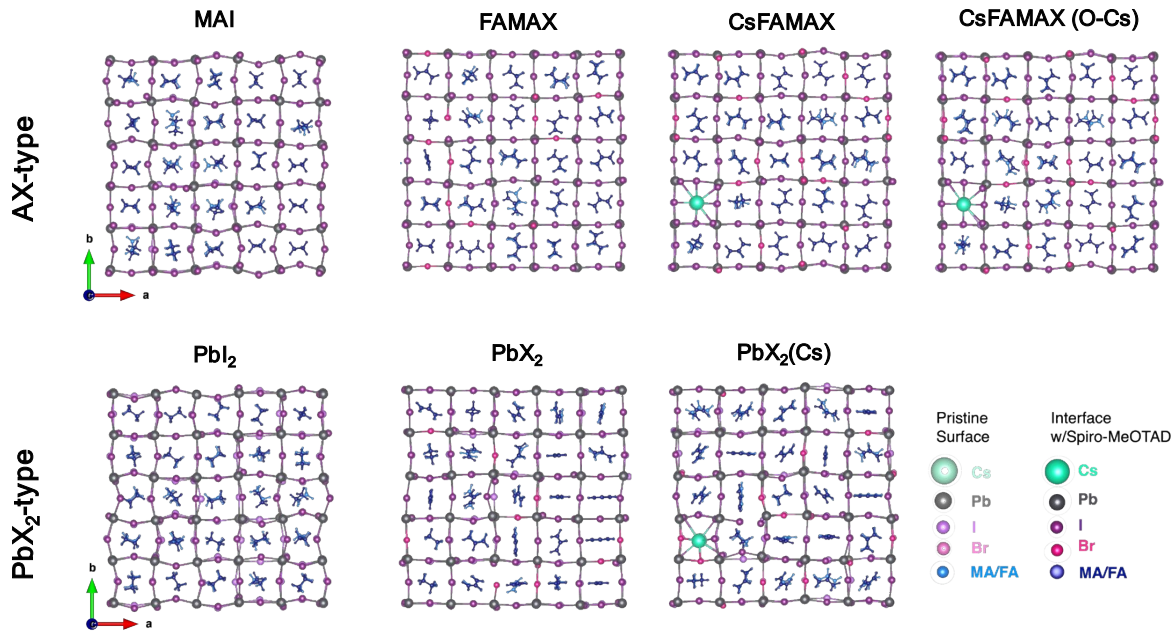

Figure S5: Structural modifications occurring in the topmost perovskite layer upon interface formation for both AX and PbX_2-type terminations.

Donor/acceptor-decomposed pDOS of all interfaces considered in this work

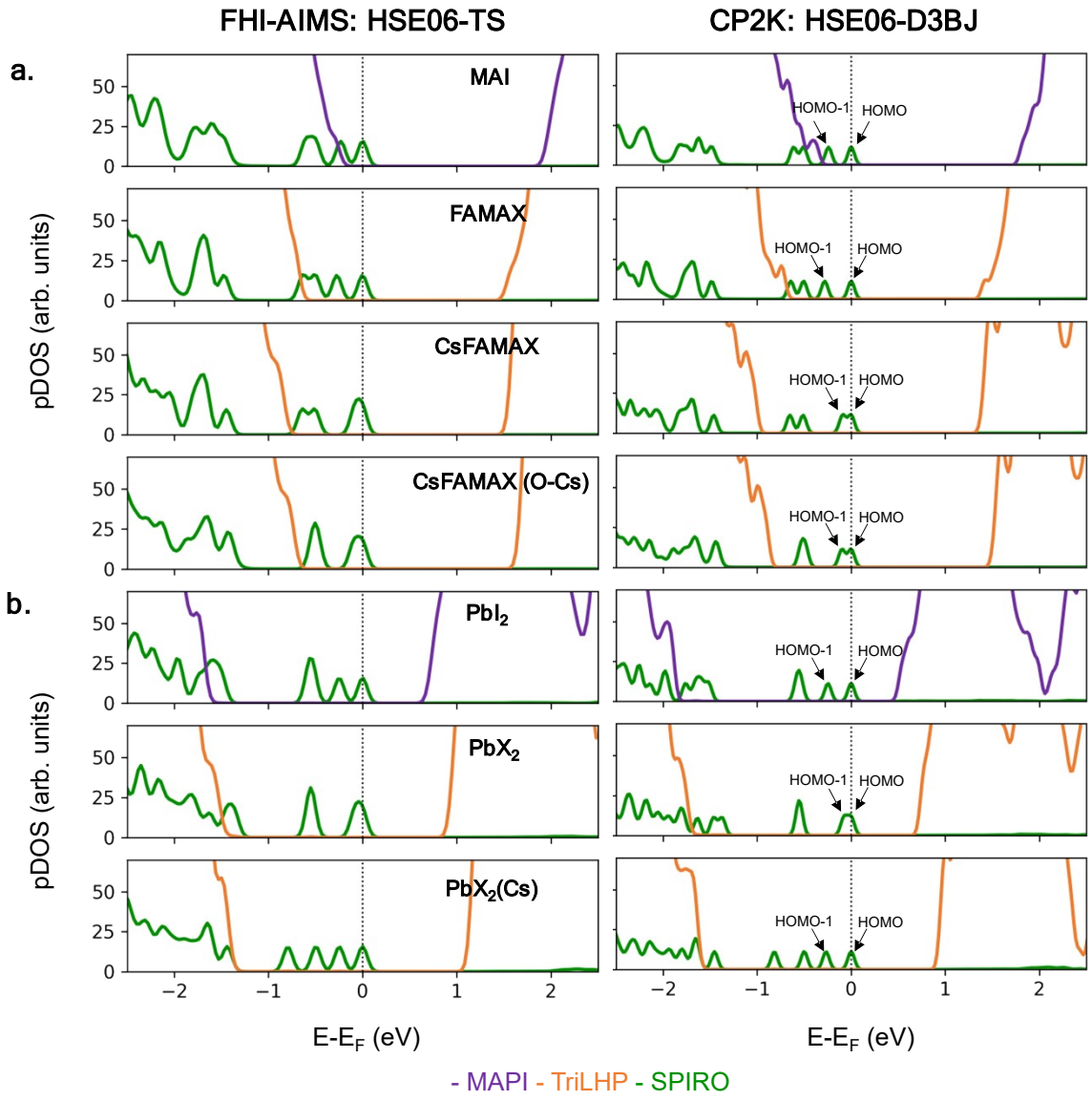

Figure S6. Density of states projected onto the interface constituents (pDOS) of MAX- (a) and PbX_2- (b) type terminations. pDOS are computed at HSE06 -TS and -D3BJ level of theory with the FHI-AIMs (right panel) and CP2K (left panel) code, respectively. Color legend: Spiro-MeOTAD (green), MAPI surfaces (violet), triLHP surfaces (orange).

Computed frontier orbitals and energetics for isolated Spiro-MeOTAD

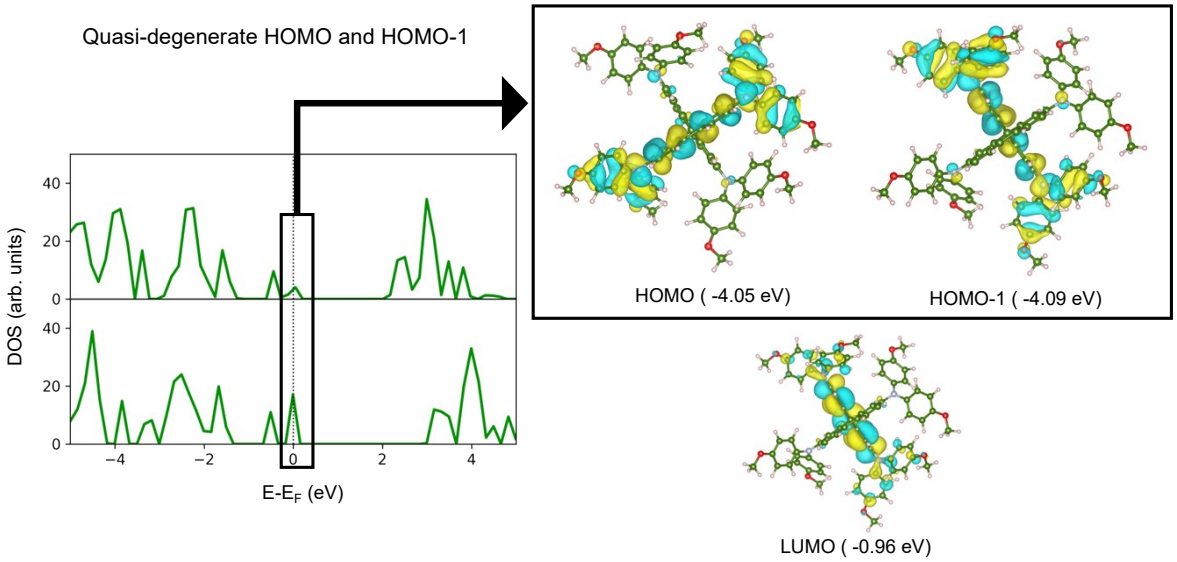

Figure S7: Total density of states calculated at PBE- (top panel) and HSE06-D3BJ (bottom panel) for isolated Spiro-MeOTAD molecule. Quasi-degenerate HOMO/HOMO-1 and LUMO of Spiro-MeOTAD molecule, calculated at HSE06-D3BJ level of theory.

Detailed view of triLHP CsFAMAX/Spiro and CsFAMAX(O-Cs)/Spiro interfaces

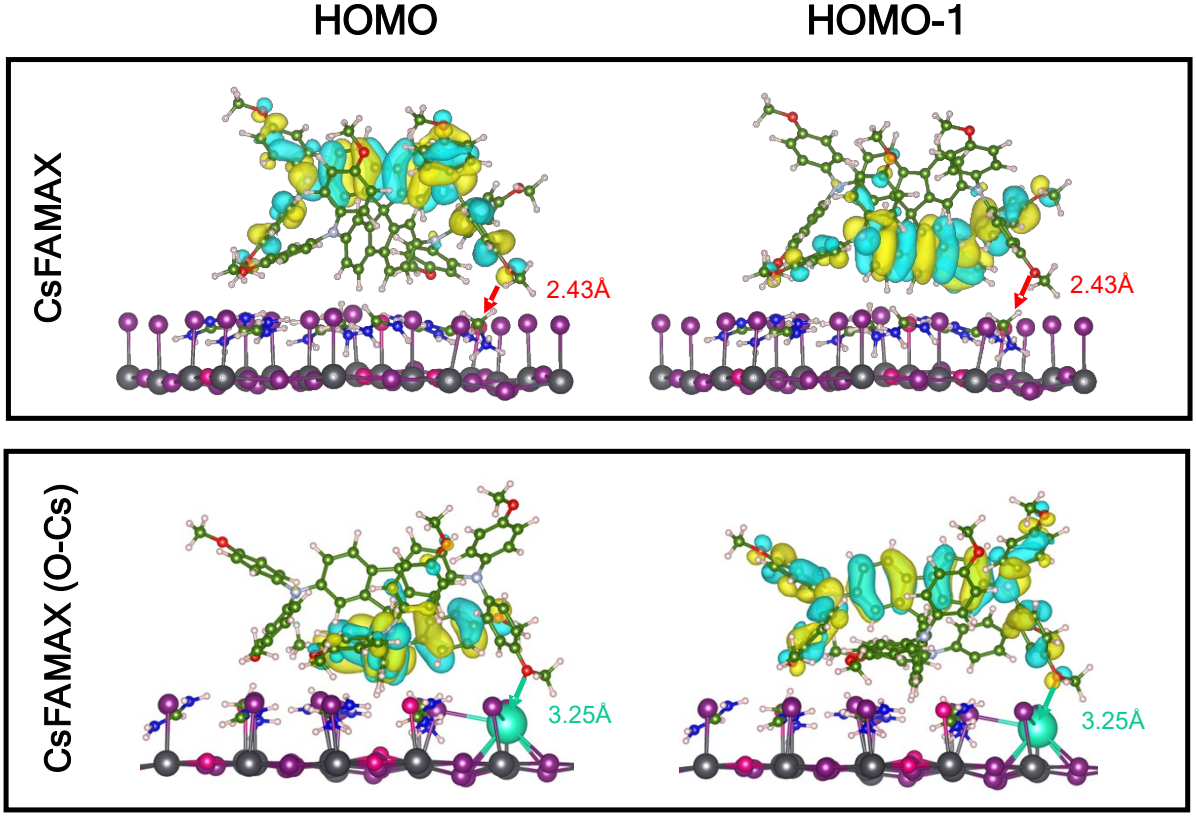

Figure S8: Spiro-MeOTAD HOMO and HOMO-1 at CsFAMAX/Spiro and CsFAMAX(O-Cs)/Spiro interfaces calculated at HSE06-D3BJ level of theory.

References

[S1] K. Burke, *J. Chem. Phys.,* 2012, **136**, 150901.

[S2] V. Havu, V. Blum, P. Havu and M. Scheffler, *J. Comput. Phys*., 2009, **228**, 8367–8379.

[S3] V. Blum, R. Gehrke, F. Hanke, P. Havu, V. Havu, X. Ren, K. Reuter and M. Scheffler, *Comput. Phys. Commun.*, 2009, **180**, 2175–2196.

[S4] E. van Lenthe, A. van der Avoird and P.E.S. Wormer, *J. Chem. Phys*., 1998, **108**, 4783–4796.

[S5] J.P. Perdew, K. Burke and Y. Wang, *Phys. Rev. B*, 1996, **54**, 16533–16539.

[S6] J.P. Perdew, K. Burke and Y. Wang, [Erratum: *Phys. Rev. B*, 1996, **54**, 16533–16539] *Phys. Rev. B*, 1998, **57**, 14999–14999.

[S7] A. Tkatchenko and M. Scheffler, *Phys. Rev. Lett.,* 2009, **102**, 073005.

[S8] J. Heyd J, G.E. Scuseria, M. Ernzerhof *J. Chem. Phys.* 2003, **118**, 8207.; J. Heyd, G.E. Scuseria, M. Ernzerhof *J. Chem. Phys.* 2006, **124**, 219906E.

[S9] Z. Futera and J. Blumberger, *J. Phys. Chem. C*, 2017, **121**, 19677–19689.

[S10] T. D. Kühne, M. Iannuzzi, M. Del Ben, V.V. Rybkin, P. Seewald, F. Stein, T. Laino, R. Z. Khaliullin, O. Schütt, F. Schiffmann, D. Golze, J. Wilhelm, S. Chulkov, M. H. Bani-Hashemian, V. Weber, U. Borštnik, M. Taillefumier, A. S. Jakobovits, A. Lazzaro, H. Pabst, T. Müller, R. Schade, M. Guidon, S. Andermatt, N. Holmberg, G.K. Schenter, A. Hehn, A. Bussy, F. Belleflamme, G. Tabacchi, A. Glöß, M. Lass, I. Bethune, C. J. Mundy, C. Plessl, M. Watkins, J. VandeVondele, M. Krack and J. Hutter*, J. Chem. Phys.* 2020, **152**, 194103.

[S11] M. I. Saidaminov, J. Kim, A. Jain, R. Quintero-Bermudez, H. Tan, G. Long, F. Tan, A. Johnston, Y. Zhao, O. Voznyy and E. H. Sargent, *Nat. Energy*, 2018, **3**, 648–654.

[S12] J. Xu, C. C. Boyd, Z. J. Yu, A. F. Palmstrom, D. J. Witter, B. W. Larson, R. M. France, J. Werner, S. P. Harvey, E. J. Wolf, W. Weigand, S. Manzoor, M. F. A. M. van Hest, J. J. Berry, J. M. Luther, Z. C. Holman and M. D. McGehee, *Science*, 2020, **367**, 1097–1104.

[S13] Y. Saygili, H.-S. Kim, B. Yang, J. Suo, A. B. Muñoz-García, M. Pavone and A. Hagfeldt, *ACS Energy Lett.*, 2020, **5**, 1271–1277.

[S14] A. Pecoraro, A. D. Maria, P. D. Veneri, M. Pavone and A. B. Muñoz-García, *Phys. Chem. Chem. Phys.*, 2020, **22**, 28401–28413.

[S15] C. Quarti, F. De Angelis and D. Beljonne, *Chem. Mater.*, 2017, **29**, 958–968.

[S16] J. Haruyama, K. Sodeyama, L. Han and Y. Tateyama *J. Phys. Chem. Lett.* 2014, **5**, 2903-2909

[S17] C. Coppola, A. Pecoraro, A. B. Muñoz-García, R. Infantino, A. Dessì, G. Reginato, R. Basosi, A. Sinicropi and M. Pavone, *Phys. Chem. Chem. Phys.*, 2022, **24**, 14993–15002.

[S18] A. Torres and L. G. C. Rego, *J. Phys. Chem. C*, 2014, **118**, 26947–26954..